

Magnetic Properties of 1:4 Complexes of $Co^{II}X_2$ (X = NCO^-, NCS^-, and Br^-) with 4-(*N*-*tert*-Butylaminoxyl)pyridine. Antiferromagnets in Crystalline States and Single-Molecule Magnets in Frozen Solutions

Shinji Kanegawa,[1] Satoru Karasawa,[1] Motohiro Nakano,[2] and Noboru Koga*[1]

[1]Graduate School of Pharmaceutical Sciences, Kyushu University, 3-1-1 Maidashi, Higashi-ku, Fukuoka 812-8582

[2]Department of Applied Chemistry, Graduate School of Engineering, Osaka University, 2-1 Yamadaoka, Suita, Osaka 565-0871

Received October 3, 2005; E-mail: koga@fc.phar.kyushu-u.ac.jp

Three cobalt(II) complexes, $[Co(X)_2(\mathbf{4NOpy})_4]$ (X = NCO^-, NCS^-, and Br^-; **4NOpy** = 4-(*N*-*tert*-butylaminoxyl)-pyridine) were prepared, and their molecular structures were characterized by X-ray structure analysis. The molecular geometry of $[Co(X)_2(\mathbf{4NOpy})_4]$ (X = NCO^- and NCS^-) is a compressed octahedron, in which the counter ions occupy the apical positions with short bond distances of 2.064–2.098 Å. In the crystalline state, from plots of χ_{mol} vs T and χ'_{mol} vs T, $[Co(NCO)_2(\mathbf{4NOpy})_4]$ and $[Co(NCS)_2(\mathbf{4NOpy})_4]$ are antiferromagnets with $T_N = 4.5$ and 15 K, respectively. In frozen solution, on the other hand, both complexes and $[Co(Br)_2(\mathbf{4NOpy})_4]$ functioned as single-molecule magnets. The χ''_{mol} vs T plot for $[Co(Br)_2(\mathbf{4NOpy})_4]$ gave a effective activation barrier (U_{eff}) of 20 K for the reorientation of the spin. From the field dependence of magnetization at various temperatures below 5 K for $[Co(X)_2(\mathbf{4NOpy})_4]$ (X = NCO^-, NCS^-, and Br^-) the values of the zero-field splitting parameters, D/k_B, were estimated to be -14, -9.7, and -4.5 K with $S = 5/2$, respectively. Theoretical studies based on the ligand-field theory model for $[Co(NCO)_2(\mathbf{4NOpy})_4]$ gave an exchange coupling parameter, J/k_B, of 29 K and a thermodynamic activation barrier, U, of 60 K.

Single-molecule magnets (SMM)s[1–3] exhibiting slow spin relaxation are of interest because they are only a few nanometers in size and have some quantum size effects. To construct a SMM, we used a heterospin system[4–6] consisting of 3d spins from a metal ion and 2p spins from organic radicals coupled magnetically through a linker. Slow relaxation for the reorientation of the spin in SMM can be understood by using a double-well energy potential diagram, in which the positive and negative M_s quantum levels are separated by a thermodynamic activation barrier (U) corresponding to $|DS^2|$, where D (<0) is a zero-field splitting parameter and S is a spin quantum number. In the heterospin complex, the metal ion and the high-spin organic species mainly contribute to a large D and S, respectively. Based on this strategy, the 1:4 complexes of $Co(NCS)_2$ with (4-pyridyl)phenylcarbene, **C1py**, and $Co(NCO)_2$ with 4-(*N*-*tert*-butylaminoxyl)pyridine, **4NOpy**, were prepared (Chart 1), and both have the SMM behavior with $U_{eff} = 89$ and 50 K, respectively, in frozen solutions.[5]

In most of the polynuclear complexes reported to be SMMs to date, the spin centers (metal ions) are surrounded by bulky diamagnetic ligands. Therefore, their spin centers are magnetically isolated even in the crystalline state. In our heterospin complex, on the other hand, the spin centers of organic radicals are located at peripheral positions of the complex and easily come close to each other intermolecularly. Actually, short contacts (<4 Å) between the organic spin center and the neighboring aromatic ligands within are often observed in the crystal structure of many heterospin complexes.[6] In order to observe the SMM behavior of $[Co(X)_2(\mathbf{4NOpy})_4]$, solutions were frozen to avoid the intermolecular interactions. Although intermolecular interactions caused by the short contacts are undesirable for SMM, the short contacts can be regarded as the formation of an additional spin network through the intermolecular interaction. Especially, a low-dimensional assembly of SMM having a uniaxial anisotropy is expected to have a unique magnetism. For example, single-chain magnets[7] and anisotropic metal complexes in a low-dimensional structure[8] have been reported to exhibit the characteristic magnetic behavior due to the structural and local metal ion anisotropies.

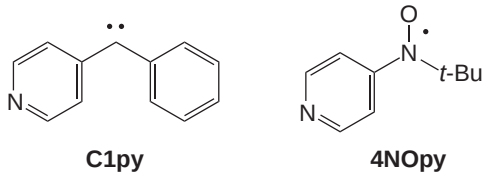

C1py **4NOpy**

Chart 1.

In this report, the magnetic properties of high-spin cobalt(II) complexes, $[Co(X)_2(\mathbf{4NOpy})_4]$ (X = NCO^- and NCS^-) in the crystalline state were investigated. In addition, to understand the magnetic properties of monometallic SMMs in frozen solution in more detail, a theoretical analysis for $[Co(NCO)_2(\mathbf{4NOpy})_4]$ was carried out, and the influence of the axial ligands (counter ions) on the SMM magnetic property in a series of cobalt complexes, $[Co(X)_2(\mathbf{4NOpy})_4]$ (X = NCO^-, NCS^-, and Br^-), was investigated.

Results and Discussion

Preparations. The pyridine ligand, **4NOpy**, having a persistent aminoxyl radical was prepared by using the reported

Published on the web September 5, 2006; doi:10.1246/bcsj.79.1372

procedure.[6b] Although **4NOpy** is unstable in the solid state, it is stabilized when coordinated to a metal ion, and the resulting metal complex is stable in air. High-spin cobalt(II) complexes, $[Co(X)_2(\mathbf{4NOpy})_4]$ ($X = NCO^-$, NCS^-, and Br^-) were prepared by mixing a solution of **4NOpy** and the corresponding cobalt(II) complex at room temperature. $[Co(NCO)_2(\mathbf{4NOpy})_4]$ and $[Co(NCS)_2(\mathbf{4NOpy})_4]$ were crystallized from Et_2O/*n*-hexane and CH_2Cl_2/*n*-hexane, respectively, at −14 °C to afford dark red crystals. After recrystallization from ether, $[Co(Br)_2(\mathbf{4NOpy})_4]$ was obtained as a brown powder containing a small amount of red brick-like single crystals under similar conditions. Based on elemental analysis, both powder and crystalline samples of $[Co(Br)_2(\mathbf{4NOpy})_4]$ were the same and, therefore, were used for SQUID measurement in frozen solution and an X-ray structure analysis, respectively. Because the amount of the crystals of $[Co(Br)_2(\mathbf{4NOpy})_4]$ was not enough for SQUID measurements, only the results using a frozen solution will be reported in this paper.

Crystal Structure Analysis. Single crystals of $[Co(NCO)_2(\mathbf{4NOpy})_4]$, $[Co(NCS)_2(\mathbf{4NOpy})_4]$, and $[Co(Br)_2(\mathbf{4NOpy})_4]$ were analyzed by an X-ray crystal structure analysis. The three complexes have similar hexa-coordinated structures, in which each cobalt ion is surrounded with four nitrogen atoms of pyridine rings (N_{Py}) at the basal plane and two counter ions at the apical positions. The molecular geometry of $[Co(NCO)_2(\mathbf{4NOpy})_4]$ and $[Co(NCS)_2(\mathbf{4NOpy})_4]$ is a compressed octahedron with a center of symmetry at the cobalt ion and with no symmetry, respectively. The ORTEP drawing of the molecular structure of $[Co(NCS)_2(\mathbf{4NOpy})_4]$ is shown in Fig. 1.

In the octahedral structure of $[Co(NCO)_2(\mathbf{4NOpy})_4]$ and $[Co(NCS)_2(\mathbf{4NOpy})_4]$, the bond lengths between the axial ligand and the cobalt ion are shorter by 0.055–0.140 Å than those between the nitrogen of pyridine and the cobalt ion (Co–N_{Py}): Co–N_{NCO} = 2.064(5) Å for $[Co(NCO)_2(\mathbf{4NOpy})_4]$ and Co–N_{NCS} = 2.088 and 2.098 Å for $[Co(NCS)_2(\mathbf{4NOpy})_4]$. On the other hand, the crystal of $[Co(Br)_2(\mathbf{4NOpy})_4]$ consists of three different molecules with slightly different geometry. The Co–Br bond lengths are longer by ca. 0.4 Å than those of Co–N_{Py}. In the three complexes, the dihedral angles between the aminoxyl plane and the pyridine ring are 6–33°, suggesting that magnetic coupling between the aminoxyl radicals and the cobalt(II) ion through the pyridine ring effectively takes place. The dihedral angle between the pyridine ring and the *XY* plane defined by the nitrogen atoms of four pyridines are 61.44 and 55.39° for $[Co(NCO)_2(\mathbf{4NOpy})_4]$, 40.24–69.11° for $[Co(NCS)_2(\mathbf{4NOpy})_4]$, and 44.55–64.15° for $[Co(Br)_2(\mathbf{4NOpy})_4]$. Selected bond lengths and dihedral angles for $[Co(NCO)_2(\mathbf{4NOpy})_4]$, $[Co(NCS)_2(\mathbf{4NOpy})_4]$, and $[Co(Br)_2(\mathbf{4NOpy})_4]$ are summarized in Table 1.

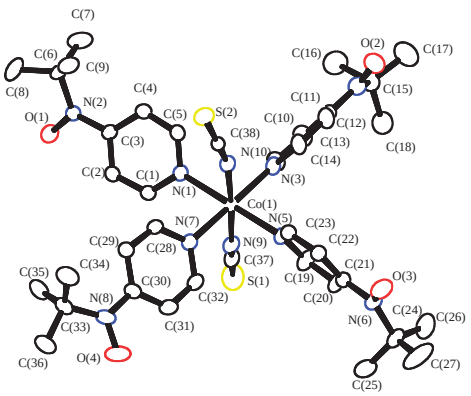

Fig. 1. ORTEP drawing of the molecular structure showing atom labeling of $[Co(NCS)_2(\mathbf{4NOpy})_4]$. Hydrogen atoms and a molecule of CH_2Cl_2 were omitted for clarity.

The crystal packings for $[Co(NCO)_2(\mathbf{4NOpy})_4]$ and $[Co(NCS)_2(\mathbf{4NOpy})_4]$ are shown in Fig. 2, in which the short contacts are indicated by arrows. In $[Co(NCO)_2(\mathbf{4NOpy})_4]$, short distances are not observed between the aminoxyl radical centers but between the radical center and the β carbon of the pyridine ring of the neighboring molecules (O2–C4′ = 3.157 Å) to form the 2D plane along the *bc* plane, Fig. 2a. Short distances between the planes (O1′–C2′ = 3.414 Å) were also observed, suggesting the formation of a 3D network, Fig. 2b. On the other hand, $[Co(NCS)_2(\mathbf{4NOpy})_4]$ has a short contact between the aminoxyl radical centers (O4–O4′ = 3.323 Å) to form a linear dimer structure, and the short distances between the dimers (O1–C14′ and O3–C1′ = 3.076 and 3.428 Å) led to the formation of a ribbon structure. The shortest distance between the ribbons is 4.977 Å, suggesting that the ribbon structures are magnetically isolated. The observed differences in the crystal structures affect the magnetic properties of both complexes in the crystalline state (vide infra).

Magnetic Properties. ESR Spectroscopy: ESR spectra of the crystalline and solution samples (≈1 mM) of $[Co(NCS)_2(\mathbf{4NOpy})_4]$ were measured in the temperature range of 300–6 K. Both crystalline and solution samples of $[Co(NCS)_2(\mathbf{4NOpy})_4]$ showed no significant signals over the entire temperature range. Under similar conditions, $[Co(NCS)_2(py)_4]$, which has no aminoxyl, showed a broad signal at $g \approx 4$ below 50 K, which is similar to that reported previously for the high-spin Co^{II} having a ground state with an effective spin of $S' = 1/2$.[9] The effective spin doublet ($S' = 1/2$) arises from the $^4T_{1g}$ ground state of Co^{II} that splits into $^4A_{2g}$ and ^4E_g in axial symmetry, and then, the lower lying state splits by spin–orbit coupling into two Kramers doublets.[10] The lack of a signal for $[Co(NCS)_2(\mathbf{4NOpy})_4]$ may, therefore, be due to extreme broadening of the absorption arising from a fast relaxation process.

SQUID Measurements: The magnetic properties of $[Co(NCO)_2(\mathbf{4NOpy})_4]$ and $[Co(NCS)_2(\mathbf{4NOpy})_4]$ were investigated in crystalline and frozen solution conditions. In the frozen solution sample, a solution of $[Co(Br)_2(\mathbf{4NOpy})_4]$ was also measured for investigation of the influence of the axial ligand on the SMM property.

In Crystalline State; The dc magnetic susceptibility measurements for pulverized samples of $[Co(NCO)_2(\mathbf{4NOpy})_4]$ and $[Co(NCS)_2(\mathbf{4NOpy})_4]$ at the constant field of 5 kOe in the temperature range of 2–300 K were performed by using a SQUID magneto/susceptometer. Temperature dependence of the molar magnetic susceptibilities (χ_{mol}) of $[Co(NCO)_2(\mathbf{4NOpy})_4]$ and $[Co(NCS)_2(\mathbf{4NOpy})_4]$ are shown as a plot of $\chi_{mol}T$ vs T in Fig. 3a.

The $\chi_{mol}T$ values at 300 K are 4.95 and 5.35 $cm^3\,K\,mol^{-1}$ for $[Co(NCO)_2(\mathbf{4NOpy})_4]$ and $[Co(NCS)_2(\mathbf{4NOpy})_4]$, respectively, and they correspond to one high-spin Co^{II} ion ($S = 3/2$) and four aminoxyls ($S = 1/2$) with significant orbital

Table 1. Selected Bond Lengths (Å) and Dihedral Angles (°) for $[Co(NCO)_2(\mathbf{4NOpy})_4]$, $[Co(NCS)_2(\mathbf{4NOpy})_4]$, and $[Co(Br)_2(\mathbf{4NOpy})_4]$

$[Co(NCO)_2(\mathbf{4NOpy})_4]$		$[Co(NCS)_2(\mathbf{4NOpy})_4]$		$[Co(Br)_2(\mathbf{4NOpy})_4]$	
Bond Lengths/Å					
Co–N(1)	2.203	Co–N(1)	2.170	Co(1)–N(1)	2.164
Co–N(3)	2.207	Co–N(3)	2.154	Co(1)–N(3)	2.215
Co–N(5)	2.064	Co–N(5)	2.168	Co(1)–Br(1)	2.611
		Co–N(7)	2.153	Co(2)–N(5)	2.238
		Co–N(9)	2.098	Co(2)–N(7)	2.152
		Co–N(10)	2.088	Co(2)–N(9)	2.241
				Co(2)–N(11)	2.174
				Co(2)–Br(2)	2.659
				Co(2)–Br(3)	2.626
				Co(3)–N(13)	2.213
				Co(3)–N(15)	2.188
				Co(3)–Br(4)	2.585
Dihedral Angles (°) between Pyridine Ring and XY Plane					
CoN(1)N(3)-N(1)C(2)C(4)	61.339	N(1)N(3)N(5)N(7)-N(1)C(2)C(4)	47.751	Co(1)N(1)N(3)-N(1)C(2)C(4)	47.138
CoN(1)N(3)-N(3)C(11)C(13)	54.877	N(1)N(3)N(5)N(7)-N(3)C(11)C(13)	58.971	Co(1)N(1)N(3)-N(3)C(11)C(13)	59.070
		N(1)N(3)N(5)N(7)-N(5)C(20)C(22)	60.093	N(5)N(7)N(9)N(11)-N(5)C(20)C(22)	78.466
		N(1)N(3)N(5)N(7)-N(7)C(29)C(31)	40.251	N(5)N(7)N(9)N(11)-N(7)C(29)C(31)	49.726
				N(5)N(7)N(9)N(11)-N(9)C(38)C(40)	56.296
				N(5)N(7)N(9)N(11)-N(11)C(47)C(49)	64.153
				Co(3)N(13)N(15)-N(13)C(56)C(58)	57.307
				Co(3)N(13)N(15)-N(15)C(65)C(67)	44.546
Dihedral Angles (°) between Pyridine Ring and Radical Plane					
N(3)C(11)C(13)-O(2)N(4)C(12)	35.337	N(1)C(2)C(5)-O(1)N(2)C(3)	20.350	N(1)C(2)C(4)-O(1)N(2)C(3)	8.407
N(1)C(2)C(4)-O(1)N(2)C(3)	10.739	N(3)C(11)C(13)-O(2)N(4)C(12)	10.140	N(3)C(11)C(13)-O(2)N(4)C(12)	14.436
		N(5)C(20)C(22)-O(3)N(6)C(21)	15.546	N(5)C(20)C(22)-O(3)N(6)C(21)	16.439
		N(7)C(29)C(31)-O(4)N(8)C(30)	6.263	N(7)C(29)C(31)-O(4)N(8)C(30)	20.941
				N(9)C(38)C(40)-O(5)N(10)C(39)	30.650
				N(11)C(47)C(49)-O(6)N(12)C(48)	5.743
				N(13)C(56)C(58)-O(7)N(14)C(57)	8.286
				N(15)C(65)C(67)-O(8)N(16)C(66)	9.687

contributions. When the temperature was lowered from 300 to 2 K, the $\chi_{mol}T$ values for $[Co(NCO)_2(\mathbf{4NOpy})_4]$ and $[Co(NCS)_2(\mathbf{4NOpy})_4]$ gradually increased, reached the maxima of 5.71 and 5.95 $cm^3\,K\,mol^{-1}$ at 30 and 100 K, and then decreased steeply down to 0.5 and 0.16 $cm^3\,K\,mol^{-1}$ at 2 K, respectively. The increase in the $\chi_{mol}T$ values observed at temperatures greater than 100 K indicates that intramolecular ferromagnetic interactions between the aminoxyl center and the cobalt ion takes place, and the steep decrease at low temperatures (<30 and 100 K for $[Co(NCO)_2(\mathbf{4NOpy})_4]$ and $[Co(NCS)_2(\mathbf{4NOpy})_4]$, respectively) may suggest that intermolecular antiferromagnetic interactions and an effect of the zero-

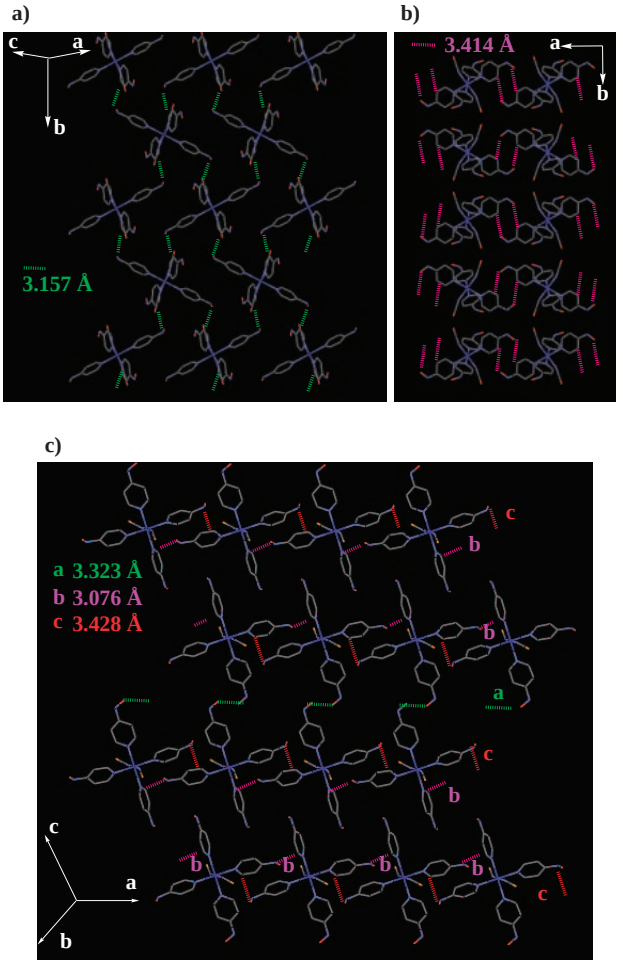

Fig. 2. Crystal packings for a), b) $[Co(NCO)_2(\mathbf{4NOpy})_4]$, and c) $[Co(NCS)_2(\mathbf{4NOpy})_4]$.

field splitting parameter caused by spin–orbit coupling in the Co^{II} ion might take place. Especially, the decrease in $\chi_{mol}T$ values from 100 K for $[Co(NCS)_2(\mathbf{4NOpy})_4]$ is due to strong antiferromagnetic interactions between the aminoxyl radical centers within a dimer. In the χ_{mol} vs T plot (Fig. 3b), a sharp maximum of χ_{mol} value at 4.5 K for $[Co(NCO)_2(\mathbf{4NOpy})_4]$ and a round one at 15 K for $[Co(NCS)_2(\mathbf{4NOpy})_4]$ were observed. The powder sample of $[Co(Br)_2(\mathbf{4NOpy})_4]$ also showed a maximum at 4.6 K in the χ_{mol} vs T plot obtained under similar conditions (Fig. S1). The maxima shifted to lower temperature when the external field was increased (5, 10, 15, and 20 kOe). The observed sharp maxima and their field dependence indicate long-range antiferromagnetic ordering.[11]

To confirm the antiferromagnetic transition, the ac magnetic susceptibilities of microcrystalline samples of $[Co(NCO)_2(\mathbf{4NOpy})_4]$ and $[Co(NCS)_2(\mathbf{4NOpy})_4]$ were measured in a zero dc field with a 5.0 Oe ac field at 500 and 1 Hz below 10 and 30 K, respectively. In-phase signals (χ'_{mol}) without frequency dependence were observed, but out-of-phase signals (χ''_{mol}) were not. Temperature dependences of the χ'_{mol} signals at 500 Hz for both complexes are shown in Fig. 3c. In the χ'_{mol} vs T plots for $[Co(NCO)_2(\mathbf{4NOpy})_4]$ and $[Co(NCS)_2(\mathbf{4NOpy})_4]$, the χ'_{mol} values gradually increased, reached a sharp and round maxima, respectively, and then decreased.

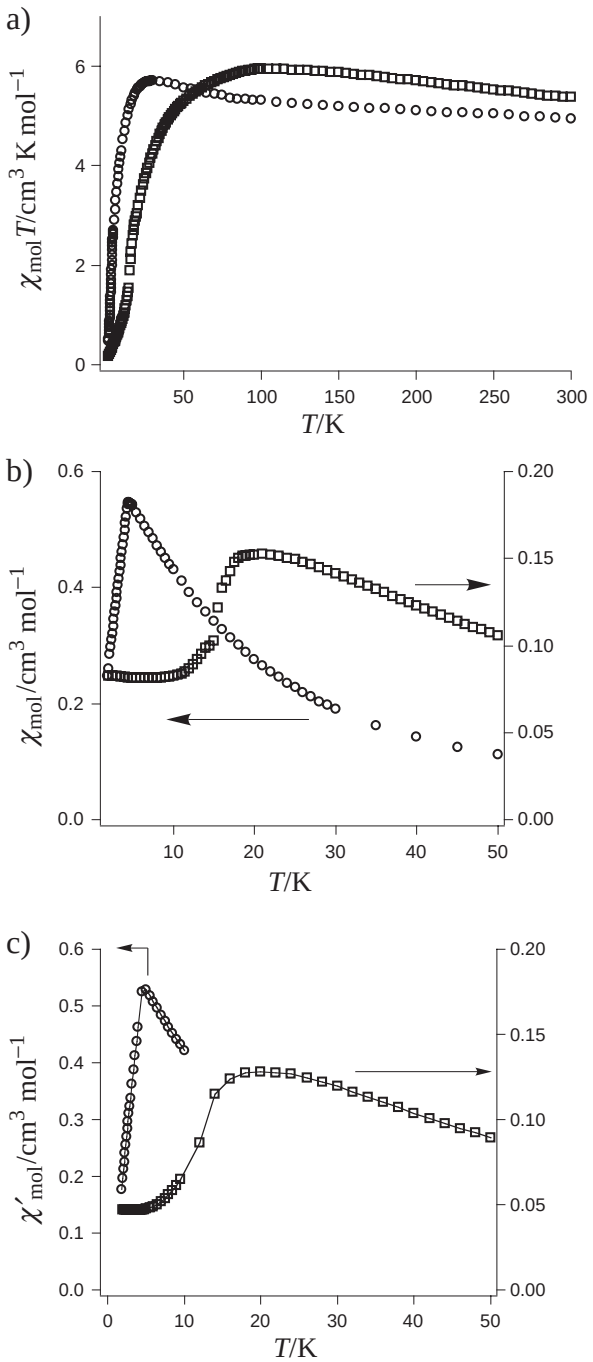

Fig. 3. Plots of a) $\chi_{mol}T$ vs T at 2–300 K, b) χ_{mol} vs T at 2–50 K, and c) χ'_{mol} vs T at 500 Hz for $[Co(NCO)_2(\mathbf{4NOpy})_4]$ (○) and $[Co(NCS)_2(\mathbf{4NOpy})_4]$ (□) in microcrystalline state. Arrows show the axis.

The temperatures at 4.5 and 15 K showing the maxima value of χ'_{mol} signal were defined as Neel temperature, T_N, for $[Co(NCO)_2(\mathbf{4NOpy})_4]$ and $[Co(NCS)_2(\mathbf{4NOpy})_4]$, respectively.

To determine the critical field, $H_c(T)$, for $[Co(NCO)_2(\mathbf{4NOpy})_4]$ and $[Co(NCS)_2(\mathbf{4NOpy})_4]$, the dc field dependence of molar magnetization, M_{mol}, was measured at several temperatures near T_N in the field range 0–50 kOe. Both complexes showed field and temperature dependencies of M_{mol} characteristic of those for antiferromagnets.[11] In the $M_{mol}/N\mu_B$ vs H

plot, where N and μ_B denote the number of complexes and the Bohr magneton, respectively, at the temperatures below T_N for $[Co(NCO)_2(\mathbf{4NOpy})_4]$, the $M_{mol}/N\mu_B$ curves showed an anomalous point (ca. 10 kOe, Fig. S2) which disappeared in the measurements above T_N. On the other hand, the $M_{mol}/N\mu_B$ vs H plot at 10 K for $[Co(NCS)_2(\mathbf{4NOpy})_4]$ showed a steep increase in the $M_{mol}/N\mu_B$ value above 45 kOe, suggesting that the critical field $H_c(T = 10\,K)$ is above 50 kOe. The $M_{mol}/N\mu_B$ vs H plots at 1.9 K for $[Co(NCO)_2(\mathbf{4NOpy})_4]$ and at 10 K for $[Co(NCS)_2(\mathbf{4NOpy})_4]$ are shown in Fig. 4a and its inset, respectively. In order to determine the value of $H_c(T)$ for $[Co(NCO)_2(\mathbf{4NOpy})_4]$, the ac magnetic susceptibilities at five temperatures, 1.9, 2.5, 3.0, 3.5, and 4.0 K, were measured in the field of 0–50 kOe (Fig. 4b). The fields at the maximum value of χ'_{mol} are 9.8–10 kOe at 1.9, 2.5, 3.0, and 3.5 K and 8.0 kOe at 4.0 K. By extrapolation, the limiting critical field, $H_c(T = 0\,K)$ is estimated to be 10 kOe. As indicated by the broken line in Fig. 4, the value of $H_c(T = 0\,K)$ obtained from the maximum of χ'_{mol} is consistent with the field of the anomalous point. In both dc and ac measurements for $[Co(NCO)_2(\mathbf{4NOpy})_4]$, the second anomalous point,[12] which indicates the transition from a spin-flop phase to a paramagnetic phase, was not clearly observed.

From X-ray crystal structure analysis, $[Co(NCO)_2(\mathbf{4NOpy})_4]$ has short contacts between the aminoxyl center and the β carbon of the neighboring pyridines ($O_{radical}\cdots C_\beta$ = 3.157 and 3.414 Å) to form a 3D network. The magnetic behavior of the antiferromagnet might be caused by an antiferromagnetic 3D-spin network. The close proximity of $O_{radical}$ to C_β has been found in the crystals of analogous complexes, $[M(hfac)_2(\mathbf{4NOpy})_2]$ (M = Mn^{II},[6a] Fe^{II}, Co^{II}, Ni^{II}, and Cu^{II},[6b] and hfac = hexafluoroacetylacetonato), that also have the antiferromagnetic interactions between molecules. The metal complexes containing anisotropic Co, Ni, and Fe ions, also, produce sharp maxima for the χ_{mol} value in the χ_{mol} vs T plots.[13] On the other hand, $[Co(NCS)_2(\mathbf{4NOpy})_4]$ showed the antiferromagnet-like behavior similar to that for $[Co(NCO)_2(\mathbf{4NOpy})_4]$. However, it has a different crystal packing in which the aminoxyl centers in two molecules are arranged with $O_{radical}\cdots O_{radical}$ = 3.323 Å and form a linear dimer structure. Furthermore, the dimer contacts other dimers with $O_{radical}\cdots C_\alpha$ distances of 3.076 and 3.428 Å forming a ribbon structure along the a axis (see Fig. 2c). Although the magnetic couplings for the inter-dimer ($O_{radical}\cdots C_\alpha$) are expected to be ferromagnetic, strong antiferromagnetic couplings between the aminoxyl centers ($O_{radical}\cdots O_{radical}$) predominantly operate and appear as the decrease in the χ_{mol} value below 100 K in the χ_{mol} vs T plot for $[Co(NCS)_2(\mathbf{4NOpy})_4]$ together with a zero-field splitting effect.

In Frozen Solution; In order to eliminate the intermolecular interactions, the magnetic measurements on frozen solutions of the complexes were carried out. The molecular structures of the complexes formed in frozen solutions were confirmed to be octahedral by the temperature dependence of the Vis spectra. Solutions (5, 10, and 15 mM, 150 µL) of the crystal of $[Co(X)_2(\mathbf{4NOpy})_4]$ (X = NCO^- and NCS^-) and the powder of $[Co(Br)_2(\mathbf{4NOpy})_4]$ dissolved in 2-methyltetrahydrofuran (MTHF) were used for SQUID measurements.

Dc Magnetic Susceptibility Measurements. The dc magnetic susceptibilities for the frozen solution samples were measured below 30 K at the constant dc field of 5 kOe. The $\chi_{mol}T$ vs T plots of the frozen solution samples (10 mM) of $[Co(X)_2(\mathbf{4NOpy})_4]$ (X = NCO^-, NCS^-, and Br^-) are shown in Fig. 5

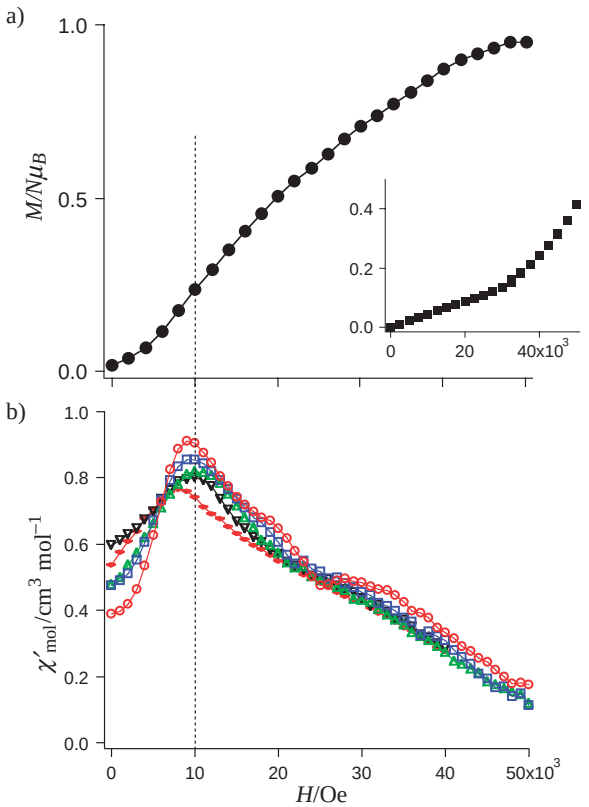

Fig. 4. Field dependence of a) dc magnetization at 1.9 K for $[Co(NCO)_2(\mathbf{4NOpy})_4]$, (●), and at 10 K for $[Co(NCS)_2(\mathbf{4NOpy})_4]$, (■; Inset) and b) In-phase signal, χ', of $[Co(NCO)_2(\mathbf{4NOpy})_4]$ at 1.9 (○), 2.5 (□), 3.0 (△), 3.5 (▽), and 4.0 (◇) K. Broken line indicates a limiting critical field, $H_c(T)$ for $[Co(NCO)_2(\mathbf{4NOpy})_4]$.

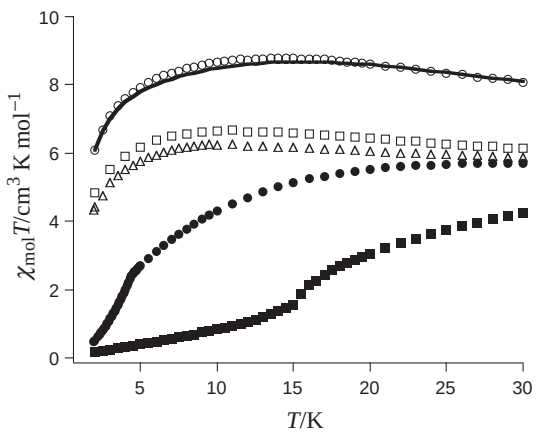

Fig. 5. $\chi_{mol}T$ vs T plot of $[Co(NCO)_2(\mathbf{4NOpy})_4]$ (○), $[Co(NCS)_2(\mathbf{4NOpy})_4]$ (□), and $[Co(Br)_2(\mathbf{4NOpy})_4]$ (△) in frozen solution (open) and in crystalline (filled). The solid line for $[Co(NCO)_2(\mathbf{4NOpy})_4]$ was fitted based on the ligand field theory model; see the text for the fitting parameters.

together with those for the crystalline sample in the corresponding temperature region.

For $[Co(NCO)_2(\mathbf{4NOpy})_4]$ and $[Co(NCS)_2(\mathbf{4NOpy})_4]$, the magnetic behavior due to the antiferromagnets observed in the crystalline state completely disappeared. The large differences in the thermal profile of the $\chi_{mol}T$ values between the crystalline and the frozen solution states clearly indicated that the intermolecular antiferromagnetic interactions observed in the crystalline states were effectively eliminated, and the complexes in the frozen solution condition were magnetically isolated. The $\chi_{mol}T$ values at 30 K are 8.1, 6.2, and 5.9 $cm^3\,K\,mol^{-1}$ for $[Co(X)_2(\mathbf{4NOpy})_4]$, where $X = NCO^-$, NCS^-, and Br^-, respectively. The values are larger than the value of 3.6 $cm^3\,K\,mol^{-1}$ ($0.375 \times 4 + 2.1$ for $[Co(NCS)_2(py)_4]$ with $S' = 1/2$)[14] for the isolated four aminoxyl radicals and a cobalt(II) ion, which suggested that ferromagnetic interactions occur intramolecularly to form a high-spin ground state. The $\chi_{mol}T$ values slightly increased on cooling, reached maxima at 13–10 K, and then gradually decreased at the lower temperature.

The dc field dependences of the magnetization (M) of the frozen solution samples of $[Co(X)_2(\mathbf{4NOpy})_4]$ ($X = NCO^-$, NCS^-, and Br^-) were measured at 2.0, 2.5, 3.0, 4.0, and 5.0 K in the range of 0–50 kOe. The data were plotted as the reduced magnetization $M/N\mu_B$ vs H/T, which are shown in Figs. 6a, 6b, and 6c for $[Co(X)_2(\mathbf{4NOpy})_4]$, where $X = NCO^-$, NCS^-, and Br^-, respectively. In the plots of $M/N\mu_B$ vs H/T for three samples, typically large deviations from the Brillouin function[15] were observed, indicating that the zero-field splitting parameter D/k_B operated at the ground state of the complexes. The magnetization data were fitted by using a matrix-diagonalization method to a model that assumes only the ground state is populated, includes the axial zero-field splitting (DS_Z^2), and involves a full powder average. The best fit for three samples gave $S = 5/2$, $D/k_B = -14.3$, -9.65, and -4.5 K, and $g = 3.11$, 2.69, and 2.51 for $[Co(X)_2(\mathbf{4NOpy})_4]$, where $X = NCO^-$, NCS^-, and Br^-, respectively. The $|D|/k_B$ values are much larger than those for the SMM reported previously.[1,2] The large $|D|/k_B$ values, especially for $[Co(NCO)_2(\mathbf{4NOpy})_4]$, suggest that there is a strong transverse interaction leading to spin quantum tunneling.[16]

Theoretical Studies. In order to analyze the magnetic property of $[Co(NCO)_2(\mathbf{4NOpy})_4]$ quantitatively, the ligand-field theoretical model[10] was employed. Deviation from O_h symmetry partially lifts the degeneracy of Co^{II} electronic ground state $^4T_{1g}$ into $^4A_{2g}$ and ^4E_g states. The energy splitting Δ between these two electronic states is conveniently expressed by introducing an effective angular momentum $\hat{L}$ with its magnitude of $L = 1$. Then, the effective Hamiltonian is written as

$$\hat{H} = \Delta\cdot\left(\hat{L}_z^2 - \frac{1}{3}\hat{L}^2\right) - \frac{3}{2}k\lambda\hat{L}\cdot\hat{S}_0 - 2J\sum_{i=1}^{4}\hat{S}_0\cdot\hat{S}_i + \mu_B\left(-\frac{3}{2}k\hat{L} + g_e\sum_{i=0}^{4}\hat{S}_i\right)\cdot B, \quad (1)$$

where $\hat{S}_0$ and $\hat{S}_i$ (i = 1–4) are spin operators of the Co^{II} ion ($S_0 = 3/2$) and four radicals ($S_i = 1/2$), μ_B and g_e are the Bohr magneton and the Landé g factor for free electron, and

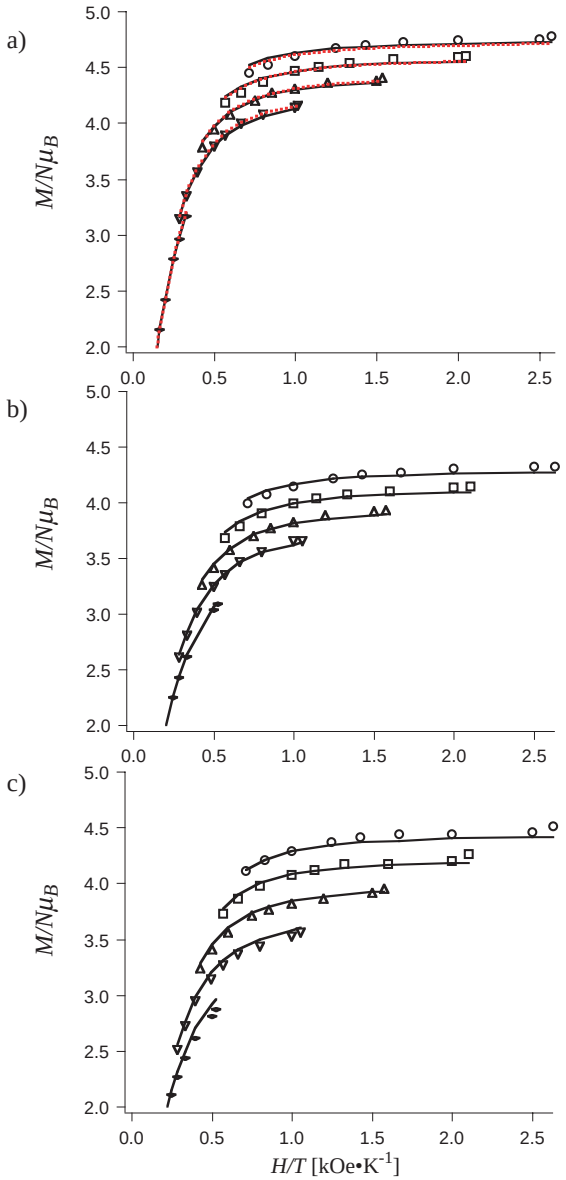

Fig. 6. $M_{mol}/N\mu_B$ vs H/T plots at 10 (◇), 20 (▽), 30 (△), 40 (□), and 50 (○) kOe for a) $[Co(NCO)_2(\mathbf{4NOpy})_4]$, b) $[Co(NCS)_2(\mathbf{4NOpy})_4]$, and c) $[Co(Br)_2(\mathbf{4NOpy})_4]$ in MTHF frozen solution. The solid lines are the fitting results and the red dashed lines in a) are those from the ligand field theory model; see the text for the fitting parameters.

parameters k, λ, and J stand for the Stevens orbital reduction factor of Co^{II}, the spin–orbit coupling of Co^{II}, and the super-exchange interaction between Co^{II} and each radical, respectively. This model is useful in analyzing the magnetic properties of isolated molecules, where intermolecular interactions are negligible. Both sets of experimental data for the plots of $\chi_{mol}T$ vs T (Fig. 5) and $M/N\mu_B$ vs H/T (Fig. 6) were simultaneously used to determine adjustable parameters Δ, k, λ, and J in the effective Hamiltonian (Eq. 1) by the nonlinear least-squares fitting based on a downhill simplex method.[17–19] Since all of the magnetic data were collected for solution samples, a powder average procedure[20] was applied to every evaluation of magnetization. The orbital reduction factor k was

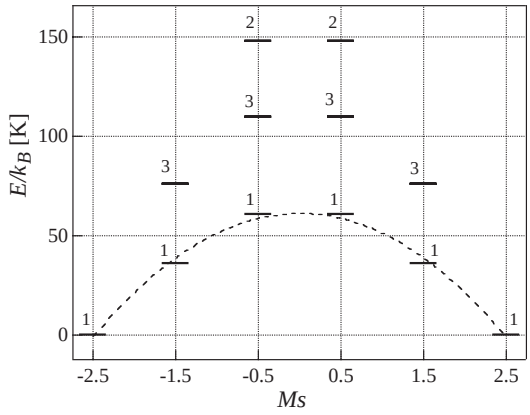

Fig. 7. E vs M_s diagram for [Co(NCO)$_2$(**4NOpy**)$_4$] obtained from optimized parameters. The broken curve is an eye-guide showing the energy-barrier profile for reversal of the resultant spin $S = 5/2$.

fixed to 1.0 to avoid overparametrization, and the optimized parameters thus obtained are $\Delta/k_B = -960$ K, $\lambda/k_B = -250$ K, and $J/k_B = 29$ K for [Co(NCO)$_2$(**4NOpy**)$_4$] and simulation curves calculated using these parameter sets are shown in Figs. 5 and 6a.

The energy level scheme corresponding to [Co(NCO)$_2$(**4NOpy**)$_4$] is shown in Fig. 7, where energy eigen values E of the Hamiltonian (Eq. 1) are plotted by levels with respective degeneracy figures against the z-component of the total spin quantum number M_S. The lowest six levels form a parabolic barrier profile with height of 60 K, partitioning $M_S = +5/2$ and $-5/2$ states. Although such a system possessing not-fully quenched orbital angular momentum cannot be described by using a zero-field splitting parameter D characteristic of the conventional Abragam–Pryce spin Hamiltonian, it was found that there exists another zero-field splitting in the ground spin manifold, which contributes to the thermodynamic activation barrier (U) for the reversal of the molecular spin. It should be noted here that the picture of the resultant molecular spin of $S = 5/2$ has a certain relevance in the low-energy region of the energy level scheme. This resultant spin value is obtained if it is assumed that a high-spin cobalt ion has a Kramers doublet ground state[10] with effective $S' = 1/2$ and ferromagnetically interacts with four surrounding radicals. This interpretation is consistent with the epr result of an analogous complex [Co(NCS)$_2$(py)$_4$], in which the ESR spectrum below 40 K resembles the one with $S' = 1/2$ and $g \approx 4$.

Since the thermodynamic activation barrier, U, obtained by the calculation is the thermal activation over the potential energy for the reversal of the spin and the effective activation barrier, U_{eff}, obtained from ac magnetic susceptibility measurements involves the quantum tunneling, the difference in the values, $U = 60$ and $U_{eff} = 50$ K, is reasonable. This difference may arise from resonance quantum tunneling.[21,22] Using $U = 60$ K, the zfs parameter $D/k_B = -10$ K for [Co(NCO)$_2$(**4NOpy**)$_4$] was estimated from the equation $U = D\{S^2 - (1/2)^2\}$ for a complex with a half-integer spin. The value of $D/k_B = -10$ K is roughly close to that (-14 K) obtained by fitting the reduced magnetization data. Although a ligand-field theory model was also applied to the dc data for [Co(NCS)$_2$(**4NOpy**)$_4$] and [Co(Br)$_2$(**4NOpy**)$_4$], it proved difficult to fit the data properly. We are currently trying to fit the data for [Co(NCS)$_2$(**4NOpy**)$_4$] and [Co(Br)$_2$(**4NOpy**)$_4$] by accounting for the decrease in orbital-angular momentum.

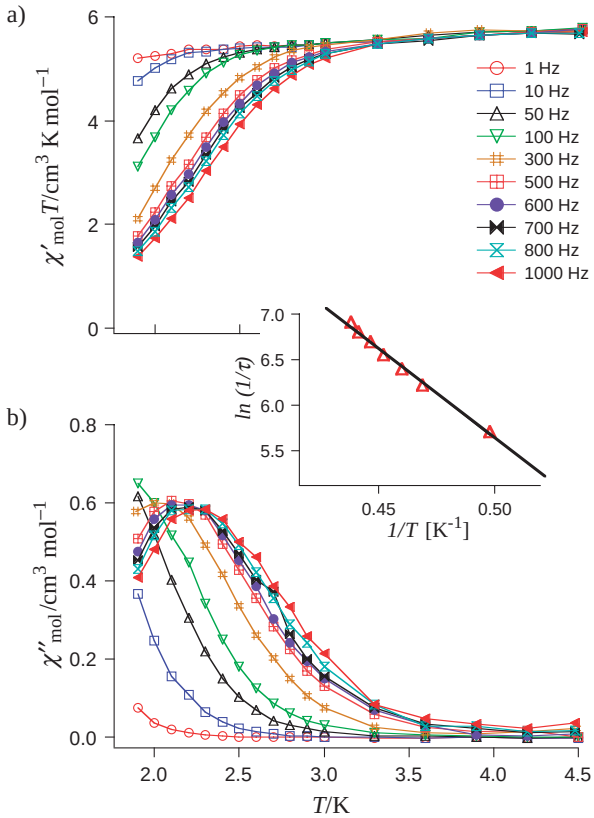

Fig. 8. a) $\chi'_{mol}T$ vs T and b) χ''_{mol} vs T plots for [Co(Br)$_2$(**4NOpy**)$_4$] in MTHF with a 5 Oe ac field oscillating at given frequencies. The solid lines are visual guides. The inset is an Arrhenius plot.

Ac Magnetic Susceptibility Measurements. To investigate the influence of the axial ligand on the activation barriers in more detail, ac magnetic susceptibility measurements on a frozen solution of [Co(Br)$_2$(**4NOpy**)$_4$] were carried out under conditions similar to those for [Co(NCO)$_2$(**4NOpy**)$_4$] and [Co(NCS)$_2$(**4NOpy**)$_4$] which were reported previously.[5a] The ac magnetic susceptibilities were measured in a zero dc field with a 5.0 Oe ac field at 1000, 800, 700, 600, 500, 100, 50, 10, 5, and 1 Hz and in the temperature range of 1.9–5.0 K. The χ'_{mol} and χ''_{mol} signals (in-phase and out-of-phase components of ac magnetic susceptibilities, respectively) with the frequency dependence were observed, indicating that the complex has a slow magnetic relaxation for the inverse of the spin. The plots of $\chi'_{mol}T$ vs T and χ''_{mol} vs T are shown in Fig. 8. In the $\chi'_{mol}T$ vs T plot, the $\chi'_{mol}T$ values decreased frequency-dependently below 3.5 K, while the χ''_{mol} signals appeared at the same temperature. In the χ''_{mol} vs T plot, maxima for the χ''_{mol} signals shifted to lower temperatures as the frequency decreased and were observed at a frequency greater than 300 Hz above 1.9 K. Since each frequency at the peak-top temperature for χ''_{mol} is consistent with $1/\tau$, the activation energy, U_{eff}, for the reversal of the spin and the pre-exponential factor, τ_0, were estimated from an Arrhenius plot of $\tau = \tau_0 \exp(U_{eff}/$

k_BT), and the values of $U_{eff} = 20$ K and $\tau_0 = 1.6 \times 10^{-7}$ s for $[Co(Br)_2(\mathbf{4NOpy})_4]$ were obtained (the inset of Fig. 8) using the peak-top temperature data above 300 Hz.

The results of the ac and dc magnetic experiments for $[Co(X)_2(\mathbf{4NOpy})_4]$ (X = NCO^-, NCS^-, and Br^-) are reproducible, and those for 5 and 15 mM samples under similar conditions showed no significant differences from the 10 mM sample. The lack of concentration effect of the magnetic behavior may rule out the possibility that slow magnetic relaxation is due to aggregation of the complex. Although it is difficult to obtain direct information about the structure of the Co^{II} complex in the frozen solution, the origin of the observed magnetic behaviors is safely concluded to be due to one isolated molecule of the Co^{II} complex (Fig. 1). The strong frequency dependences of the χ'_{mol} and χ''_{mol} signals[23] and the physically reasonable values of τ_0 suggest that these Co^{II} complexes in frozen solution function as an SMM rather than a spin glass.[24] The value of $\Delta T_f/T_f(0)\Delta(\log w)$ supports the formation of a SMM, where ΔT_f is the shift of the peak temperature in χ'_{mol}, $\log w$ is the logarithm of the applied frequency, and $T_f(0)$ is the position of the peak at zero frequency, obtained by the χ'_{mol} vs T plots. The values are 0.28, 0.36, and 0.40 for $[Co(X)_2(\mathbf{4NOpy})_4]$, where X = NCO^-, NCS^-, and Br^-, respectively. According to Mydosh's work,[25] those values are in the region $\Delta T_f/T_f(0)\Delta(\log w) > 0.2$, for a SMM.

Comparison of SMM Properties in $[Co(NCO)_2(\mathbf{4NOpy})_4]$, $[Co(NCS)_2(\mathbf{4NOpy})_4]$, and $[Co(Br)_2(\mathbf{4NOpy})_4]$. The molecular structures of $[Co(X)_2(\mathbf{4NOpy})_4]$ (X = NCO^-, NCS^-, and Br^-) in the frozen solutions are expected to be similar octahedrons, as observed in Fig. 1, in which the counter ions, X, are coordinated to the cobalt ion in a trans configuration. For the three complexes, the values of the effective activation barrier for the reorientation of the spin, the pre-exponential factors, and the zero-field splitting parameters (U_{eff}, τ_0, and D/k_B, respectively) obtained by the ac and dc magnetic susceptibility measurements are summarized in Table 2 together with those reported previously.[5a]

The values of U_{eff} depend on the axial ligands (50, 31, and 20 K, respectively), while the values of τ_0 are nearly constant ($1.6–1.8 \times 10^{-7}$ s). The U_{eff} values decrease in the order of NCO^-, NCS^-, and Br^-, suggesting that the magnitude of the $|D|/k_B$ value decreases in the same order; the thermodynamic activation barrier, $U = |D|\{S^2 - (1/2)^2\}$ in the half-integer spin system. As listed in Table 2, actually, the $|D|/k_B$ values obtained by the fitting of the reduced magnetization data decrease in the order of NCO^-, NCS^-, and Br^-. Although the study of the axial ligand effect on Co^{II} ion in detail are still underway,[26] it is worthy to note that the axial ligands in this 1:4 heterospin complex control the zero-field splitting parameter relating to the activation barrier for the reorientation of the spin in a SMM.

Conclusion

Based on the heterospin strategy for a SMM, the 1:4 cobalt–pyridine complexes, $[Co(X)_2(\mathbf{4NOpy})_4]$ (X = NCO^-, NCS^-, and Br^-) having four stable aminoxyls were prepared. These complexes with a small spin multiplicity ($S = 5/2$) functioned as antiferromagnets in the crystalline state and as SMMs with relatively large U_{eff} values in the frozen solution. Niel temperatures, T_N, for the antiferromagnets are 4.5 and 15 K for $[Co(X)_2(\mathbf{4NOpy})_4]$, where X = NCO^- and NCS^-, respectively. The magnetic properties of SMM in these complexes strongly depended on the axial ligands. The magnitude of $|D|/k_B$ values for $[Co(X)_2(\mathbf{4NOpy})_4]$ decreased in order of X = NCO^-, NCS^-, and Br^-. Since an increase in the $|D|/k_B$ value leads to an increase in the U_{eff} value, it should be possible to design the SMM having a large activation barrier in a heterospin system. The dc magnetic susceptibility data for $[Co(NCO)_2(\mathbf{4NOpy})_4]$ was analyzed by a ligand-field theory model to afford the exchange-coupling parameter $J/k_B = 29$ K and the thermodynamic activation barrier $U = 60$ K. The difference between the U value and the U_{eff} value is understood as arising from a resonant spin quantum tunneling.

The magnetic behavior of $[Co(X)_2(\mathbf{4NOpy})_4]$ was strongly affected by the magnetic anisotropy of the Co^{II} ions[27] which suggests that a single-chain magnet can be prepared by linearly connecting this type of SMM with appropriate bridging ligands. Along this idea, preparation of a new ligand having two pyridine units and organic spins is in progress.

Experimental

General Methods. Infrared spectra were recorded on a JASCO FT/IR 420 spectrometer with KBr pellets. Vis–NIR spectra were recorded on a JASCO V570 spectrometer. Melting points were obtained with a MEL-TEMP heating block and are uncorrected. Elemental analyses were performed in the Analytical Center of the Faculty of Science at Kyushu University.

X-ray Crystal and Molecular Structure Analyses. Crystallographic data and experimental details for $[Co(NCO)_2(\mathbf{4NOpy})_4]$ and $[Co(NCS)_2(\mathbf{4NOpy})_4]$ are summarized in Table 3. Suitable single crystals were glued onto a glass fiber using epoxy resin. All X-ray data were collected on a Rigaku Raxis-Rapid diffractometer with graphite monochromated Mo Kα radiation ($\lambda = 0.71069$ Å). Reflections were collected at 123 ± 1 K. The molecular structures were solved by direct methods (SIR program) and expanded using Fourier techniques (DIRDIF 99). The refinements were converged using the full-matrix least-squares method from the Crystal Structure software package[28] to give the $P2_1/c$ (No. 14), $P\bar{1}$ (No. 2), and $P2_1/n$ (No. 14) space groups for $[Co(NCO)_2(\mathbf{4NOpy})_4]$, $[Co(NCS)_2(\mathbf{4NOpy})_4]$, and $[Co(Br)_2(\mathbf{4NOpy})_4]$, respectively. All non-hydrogen atoms were refined anisotropically; hydrogen atoms were included at standard positions (C–H = 0.96 Å, C–C–H = 120°) and refined isotropically using a rigid model. Crystallograph-

Table 2. The Values of U_{eff}, τ_0, and D/k_B for $[Co(X)_2(\mathbf{4NOpy})_4]$ (X = NCO^-, NCS^-, and Br^-)

	$[Co(NCO)_2(\mathbf{4NOpy})_4]$	$[Co(NCS)_2(\mathbf{4NOpy})_4]$	$[Co(Br)_2(\mathbf{4NOpy})_4]$
U_{eff}/K	50[a)]	31[a)]	20
τ_0/s	1.8×10^{-7} [a)]	1.7×10^{-7} [a)]	1.6×10^{-7}
D/k_B/K	−14.3	−9.7	−4.5

a) Ref. 5a.

Table 3. Crystallographic Data Collection and Structural Refinement Information

	$[Co(NCO)_2(\mathbf{4NOpy})_4]$	$[Co(NCS)_2(\mathbf{4NOpy})_4]$	$[Co(Br)_2(\mathbf{4NOpy})_4]$
Empirical formula	$C_{38}H_{52}N_{10}O_6Co\cdot Et_2O$	$C_{38}H_{52}N_{10}S_2Co\cdot CH_2Cl_2$	$C_{36}H_{52}O_4N_8Br_2Co$
Formula weight	877.95	907.94	879.60
Crystal class	monoclinic	triclinic	monoclinic
Space group	$P2_1/c$ (#14)	$P\bar{1}$ (#2)	$P2_1/n$ (#14)
a/Å	11.892(4)	11.139(8)	11.7096(6)
b/Å	18.244(7)	13.35(1)	22.297(1)
c/Å	11.950(3)	17.30(1)	31.114(2)
α/deg		104.48(8)	
β/deg	115.81(2)	94.47(3)	93.578(2)
γ/deg		106.60(4)	
V/Å^3	2333.7(1)	2355.2(4)	8107.7(8)
μ/cm^{-1}	4.25	6.15	24.48
Z	2	2	8
Crystal size/mm^3	$0.3 \times 0.3 \times 0.3$	$0.6 \times 0.4 \times 0.3$	$0.45 \times 0.30 \times 0.30$
D_{calcd}/g cm^{-3}	1.249	1.298	1.441
$F(000)$	934	966	3624
Radiation	Mo Kα	Mo Kα	Mo Kα
T/K	123	123	123
No. reflections measured	21554	21325	69420
No. unique reflections	5338	10462	18177
No. reflections observed	3081 ($I > 1.00\sigma(I)$)	7215 ($I > 3.00\sigma(I)$)	12022 ($I > 1.00\sigma(I)$)
No. parameters	292	577	1026
R_1[a)]	0.049 ($I > 2.00\sigma(I)$)	0.058 ($I > 3.00\sigma(I)$)	0.065 ($I > 2.00\sigma(I)$)
wR_2[a)]	0.140 ($I > 1.00\sigma(I)$)	0.129 ($I > 3.00\sigma(I)$)	0.117 ($I > 1.00\sigma(I)$)
GOF	0.64	1.88	1.067

a) $R_1 = \Sigma||F_0| - |F_c||/\Sigma|F_0|$; $wR_2 = \{\Sigma w(F_0^2 - F_c^2)^2/\Sigma w(F_0^2)^2\}^{1/2}$.

ic data for the structure reported in this paper have been deposited with the Cambridge Crystallographic Data Centre as supplementary publication Nos. CCDC-224808, -212429, and -258046, for $[Co(NCO)_2(\mathbf{4NOpy})_4]\cdot Et_2O$, $[Co(NCS)_2(\mathbf{4NOpy})_4]\cdot CH_2Cl_2$, and $[Co(Br)_2(\mathbf{4NOpy})_4]$, respectively.

ESR Spectra Measurements. ESR spectra were recorded on a Bruker Biospin EMX EPR X-band (9.4 GHz) spectrometer. An Air Products LTD-3-110 liquid helium transfer system was attached for the low-temperature measurements. The crystalline and solution samples were placed in 5 mm o.d. quartz tubes, degassed by three freeze-and-thaw cycles, and sealed.

SQUID Measurements. Direct current (dc) and alternating current (ac) magnetic susceptibilitiy data were obtained on Quantum Design MPMS-5S and MPMS2 SQUID magneto/susceptometers, respectively, and corrected for the magnetization of the sample holder and capsule, and the diamagnetic contributions to the samples, which were estimated from Pascal's constants.[10a] A pulverized sample was prepared by grinding crystals of the complex to powder. In the frozen solution, the dc magnetic susceptibilities were obtained by subtracting the data for the solvent and the capsule from the one for the sample. The diamagnetic susceptibility (χ_{dia}) at 5 kOe for the solvent and the capsule was $-3.7--5.5 \times 10^{-4}$ cm^3 in the range of 2–30 K, which is 3.1–56% of the M value of the samples. In the ac magnetic susceptibility measurements of frozen solution samples, the raw data of the in-phase and out-of-phase (χ'_{mol} and χ''_{mol}, respectively) components were relatively small due to the low concentration of spins. However, the peak-top signal intensities obtained at 5 Oe ac field are $> 9.1 \times 10^{-6}$ and $> 3.0 \times 10^{-6}$ cm^3 for χ'_{mol} and χ''_{mol} components, respectively, which were strong enough to determine as signals.

Materials. Diethyl ether was distilled from sodium benzophenone ketyl. Dichloromethane was distilled under high-purity N_2 after drying with calcium hydride. The $Co(NO_3)_2\cdot 6H_2O$, $Co(NCS)_2$, and $CoBr_2$ were purchased and used without purification. The hydroxylaminopyridine derivative, **4NOHpy**, which is a precursor of **4NOpy**, was prepared by the reported procedure.[6b]

4-(*N*-*tert*-Butylaminoxyl)pyridine, 4NOpy: Freshly prepared Ag_2O (170 mg, 0.72 mmol) was added to a solution of the corresponding hydroxylamines, **4NOHpy**, (100 mg, 0.6 mmol),[6b] in Et_2O (or CH_2Cl_2; 10 mL) and the suspension was stirred for 2 h. After filtration, the volume of the solution of **4NOpy** was reduced to ca. 5 mL on a rotary evaporator. The obtained solution of **4NOpy** was used for the preparation of a cobalt complex without isolation.

Tetrakis[4-(*N*-*tert*-butylaminoxyl)pyridine]di(isocyanato-*N*)-cobalt(II), $[Co(NCO)_2(4NOpy)_4]$: A solution of **4NOpy** (0.6 mmol) in Et_2O (5 mL), a solution of $Co(NO_3)_2\cdot 6H_2O$ (39 mg, 0.13 mM) in EtOH (1 mL), and a solution of KNCO (22 mg, 0.27 mmol) in H_2O (1 mL) were mixed and then stirred for 10 min. The volume of the mixture was reduced to dryness under reduced pressure. The obtained dark green solid was dissolved in a small amount of CH_2Cl_2 (ca. 5 mL). Et_2O (30 mL) and *n*-hexane (15 mL) were added to the mixture, and then, the volume of the solution was reduced to 30 mL on a rotary evaporator. The resulting precipitates were removed by filtration, and the solution was kept at -14 °C. The complex $[Co(NCO)_2(\mathbf{4NOpy})_4]$ was obtained as dark red brick-like crystals (0.025 g). Mp (dec.) 108–110 °C; IR (KBr pellet) $\nu = 2206$ and 2185 cm^{-1} (NCO); Anal. Calcd for $C_{38}H_{52}N_{10}O_6Co\cdot Et_2O$: C, 57.46; H, 7.12; N, 15.95%. Found: C, 57.50; H, 7.10; N, 15.93%.

Tetrakis[4-(*N*-*tert*-butylaminoxyl)pyridine]di(thiocyanato-*N*)-

cobalt(II), [Co(NCS)$_2$(4NOpy)$_4$]: A solution of $Co(NCS)_2$ (0.19 g, 1.1 mmol) in EtOH (25 mL) and a solution of **4NOpy** (4.2 mmol) in CH_2Cl_2 (85 mL) were mixed. *n*-Hexane (70 mL) was added to the mixture, and then the volume of the solution was reduced to ca. 50 mL on a rotary evaporator. The resulting precipitates were removed by filtration and the solution was kept at −14 °C. The complex, [Co(NCS)$_2$(**4NOpy**)$_4$], was obtained as dark red brick-like crystals (0.39 g). Mp (dec.) 133–135 °C, IR (KBr pellet) $\nu = 2080$(sh) and 2067 cm^{-1} (NCS); Anal. Calcd for $C_{38}H_{52}N_{10}O_4S_2Co\cdot(CH_2Cl_2)_{0.83}$: C, 51.44; H, 5.97; N, 15.45%. Found: C, 51.41; H, 6.07; N, 15.22%.

Dibromotetrakis[4-(*N*-*tert*-butylaminoxyl)pyridine]cobalt(II), [Co(Br)$_2$(4NOpy)$_4$]: A solution of $CoBr_2$ (21.9 mg, 0.1 mmol) in Et_2O (10 mL) and a solution of **4NOpy** (0.6 mmol) in Et_2O (30 mL) were mixed. The resulting precipitates were removed by filtration, and the solution was kept at −30 °C. The complex [Co(Br)$_2$(**4NOpy**)$_4$] was obtained as a brown powder together with a small amount of the red brick-like single crystals, which is the same compound based on elemental analysis. Therefore, the complex in the former and the latter states was used as the sample for a SQUID measurement in frozen solution and an X-ray structure analysis, respectively. Mp (dec.) 102–105 °C. Anal. Calcd for $C_{36}H_{52}N_8O_4CoBr_2\cdot(Et_2O)_{0.33}$: C, 49.59; H, 6.17; N, 12.39%. Found: C, 49.43; H, 6.17; N, 12.18%.

This work was supported by a Grant-in-Aid for Scientific Research (B)(2) (No. 17350070) from the Ministry of Education, Culture, Sports, Science and Technology, Japan, and by "Nanotechnology Support Project" of the Ministry of Education, Culture, Sports, Science and Technology (MEXT), Japan. S. K. acknowledges the scholarship by Japan Society for Promotion of Science (JSPS).

Supporting Information

The plots of $\chi_{mol}T$ vs T and χ' vs T for the powder sample of [Co(Br)$_2$(**4NOpy**)$_4$] (Fig. S1) and plots of $M/N\mu_B$ vs H and dM/dH vs H at 1.9 K for [Co(NCO)$_2$(**4NOpy**)$_4$] (Fig. S2). This material is available free of charge on the web at: http://www.csj.jp/journals/bcsj/.

References

1 D. Gatteschi, R. Sessoli, *Angew. Chem., Int. Ed.* **2003**, *42*, 268.

2 a) J. Tasiopoulos, A. Vinslava, W. Wernsdorfer, K. A. Abboud, G. Christou, *Angew. Chem., Int. Ed.* **2004**, *43*, 2117. b) M. Murugesu, M. Habrych, W. Wernsdorfer, K. A. Abboud, G. Christou, *J. Am. Chem. Soc.* **2004**, *126*, 4766. c) E. K. Brechin, C. Boskovic, W. Wenrsdorfer, J. Yoo, A. Yamaguchi, E. C. Sanudo, T. R. Concolino, A. L. Rheingold, H. Ishimoto, D. N. Hendrickson, G. Christou, *J. Am. Chem. Soc.* **2002**, *124*, 9710. d) G.-O. Bian, T. Kuroda-Sowa, H. Konaka, M. Hatano, M. Maekawa, M. Munakata, H. Miyasaka, M. Yamashita, *Inorg. Chem.* **2004**, *43*, 4790. e) M. Soler, W. Wernsdorfer, K. A. Abboud, J. C. Huffman, E. R. Davidson, D. N. Hendrickson, G. Christou, *J. Am. Chem. Soc.* **2003**, *125*, 3576. f) C. Boskovic, E. K. Brechin, W. E. Streib, K. Folting, J. C. Bollinger, D. N. Hendrickson, G. Christou, *J. Am. Chem. Soc.* **2002**, *124*, 3725.

3 a) H. Oshio, N. Hoshino, T. Ito, M. Nakano, *J. Am. Chem. Soc.* **2004**, *126*, 8805. b) J. J. Sokol, A. G. Hee, J. R. Long, *J. Am. Chem. Soc.* **2002**, *124*, 7656. c) H. Andres, R. Basler, A. J. Blake, C. Cadiou, G. Chaboussant, C. M. Grant, H.-U. Güdel, M. Murrie, S. Parsons, C. Paulsen, F. Semadini, V. Villar, W. Wernsdorfer, R. E. P. Winpenny, *Chem. Eur. J.* **2002**, *8*, 4867. d) C. Boskovic, W. Wernsdorfer, K. Folting, J. C. Huffman, D. N. Hendrickson, G. Christou, *Inorg. Chem.* **2002**, *41*, 5107.

4 a) S. Karasawa, H. Kumada, N. Koga, H. Iwamura, *J. Am. Chem. Soc.* **2001**, *123*, 9685. b) S. Karasawa, N. Koga, *Polyhedron* **2003**, *22*, 1877. c) H. Morikawa, S. Karasawa, N. Koga, *Appl. Magn. Reson.* **2003**, *23*, 507. d) S. Karasawa, N. Koga, *Polyhedron* **2001**, *20*, 1387. e) H. Morikawa, F. Imamura, Y. Tsurukami, T. Itoh, H. Kumada, S. Karasawa, N. Koga, H. Iwamura, *J. Mater. Chem.* **2001**, *11*, 493.

5 a) S. Kanegawa, S. Karasawa, M. Nakano, N. Koga, *Chem. Commun.* **2004**, 1750. b) S. Karasawa, G. Zhou, H. Morikawa, N. Koga, *J. Am. Chem. Soc.* **2003**, *125*, 13676.

6 a) Y. Ishimaru, M. Kitano, H. Kumada, N. Koga, H. Iwamura, *Inorg. Chem.* **1998**, *37*, 2273. b) M. Kitano, Y. Ishimaru, K. Inoue, N. Koga, H. Iwamura, *Inorg. Chem.* **1994**, *33*, 6012. c) H. Kumada, A. Sakane, N. Koga, H. Iwamura, *J. Chem. Soc., Dalton Trans.* **2000**, 911.

7 a) S. Wang, J. Zuo, S. Gao, Y. Song, H. Zhou, Y. Zhang, X. You, *J. Am. Chem. Soc.* **2004**, *126*, 8900. b) H. Miyasaka, R. Clérac, K. Mizushima, K. Sugiura, M. Yamashita, W. Wernsdorfer, C. Coulon, *Inorg. Chem.* **2003**, *42*, 8203. c) R. Clérac, H. Miyasaka, M. Yamashita, C. Coulon, *J. Am. Chem. Soc.* **2002**, *124*, 12837. d) L. M. Toma, R. Lescouëzec, F. Lloret, M. Julve, J. Vaissermann, M. Verdaguer, *Chem. Commun.* **2003**, 1850. e) A. Caneschi, D. Gatteschi, N. Lalioti, C. Sangregorio, R. Sessoli, G. Venturi, A. Vindigni, A. Rettori, M. G. Pini, M. A. Novak, *Angew. Chem., Int. Ed.* **2001**, *40*, 1760. f) T.-F. Liu, D. Fu, S. Gao, Y.-Z. Zhang, H.-L. Sun, G. Su, Y.-J. Liu, *J. Am. Chem. Soc.* **2003**, *125*, 13976.

8 a) Z. Zhu, S. Karasawa, N. Koga, *Inorg. Chem.* **2005**, *44*, 6004. b) H. Miyasaka, H. Ieda, N. Masamoto, K. Sugiura, M. Yamashita, *Inorg. Chem.* **2003**, *42*, 3509. c) J. Larionova, O. Kahn, S. Gohlen, L. Ouahab, R. Clérac, *J. Am. Chem. Soc.* **1999**, *121*, 3349. d) J. Larionova, O. Kahn, S. Golhen, L. Ouahab, R. Clérac, *Inorg. Chem.* **1999**, *38*, 3621.

9 a) H. Jankovics, M. Daskalakis, C. P. Raptopoulou, A. Terzis, V. Tangoulis, J. Giapintzakis, T. Kiss, A. Salifouglou, *Inorg. Chem.* **2002**, *41*, 3366. b) P. Thuery, J. Zarembowitch, *Inorg. Chem.* **1986**, *25*, 2001. c) J. Zarembowitch, O. Kahn, *Inorg. Chem.* **1984**, *23*, 589.

10 a) O. Kahn, *Molecular Magnetism*, Wiley-VCH Publishers, Weinheim, **1993**. b) J. M. Herrera, A. Bleuzen, Y. Dromzée, M. Julve, F. Lloret, M. Verdaguer, *Inorg. Chem.* **2003**, *42*, 7052. c) H. Sakiyama, R. Ito, H. Kumagai, K. Inoue, M. Sakamoto, Y. Nishida, M. Yamasaki, *Eur. J. Inorg. Chem.* **2001**, 2027.

11 a) J. L. Manson, Q. Huang, J. W. Lynn, H.-J. Koo, M.-H. Whangbo, R. Bateman, T. Otsuka, N. Wada, D. N. Argyriou, J. S. Miller, *J. Am. Chem. Soc.* **2001**, *123*, 162. b) P. King, R. Clérac, C. E. Anson, C. Coulon, A. Powell, *Inorg. Chem.* **2003**, *42*, 3492. c) C. Aoki, T. Ishida, T. Nogami, *Inorg. Chem.* **2003**, *42*, 7616. d) W. R. Zhang, J. R. Jeitler, M. M. Turnbull, C. P. Landee, M. Y. Wei, R. D. Willett, *Inorg. Chim. Acta* **1997**, *256*, 183.

12 Shoulders at 20 and 35 kOe in the plot signal at 1.9 and 2.5 K were observed.

13 Unpublished results.

14 The χT value of 2.1 was obtained by the SQUID measurement of [Co(NCS)$_2$(py)$_4$] under a similar frozen solution condition. When an effective spin of $S' = 1/2$ in use for the Co^{II} ion, the value of 2.1 gave an effective g value, g_{eff}, of 4.7.

15 $M = NgS\mu_B B(x)$ where $B(x)$ is a Brillouin function, where

$x = gS\mu_B H/k_B T$, and the other symbols have their usual meanings.

16 Actually, fast relaxation of magnetization was observed in the hysteresis loop at 1.9 K for $[Co(NCO)_2(\mathbf{4NOpy})_4]$.[5b]

17 J. A. Nelder, R. Mead, *Comput. J.* **1965**, *7*, 308.

18 J. M. Parkinson, D. Hutchinson, in *Numerical Methods for Non-Linear Optimization*, ed. by F. A. Lootsma, Academic Press, London, **1972**, pp. 115–135.

19 W. H. Press, S. A. Teukolsky, W. T. Vetterling, B. P. Flannery, *Numerical Recipes*, Cambridge University Press, Cambridge, **1986**.

20 W. Gautschi, *ACM Trans. Math. Software* **1994**, *20*, 21.

21 a) J. Friedman, M. Sarachik, J. Tejada, R. Ziolo, *Phys. Rev. Lett.* **1996**, *76*, 3830. b) L. Thomas, F. Lionti, R. Ballou, D. Gatteschi, R. Sessoli, B. Barbara, *Nature* **1996**, *383*, 145.

22 a) M. Soler, W. Wernsdorfer, K. Folting, M. Pink, G. Christou, *J. Am. Chem. Soc.* **2004**, *126*, 2156. b) D. N. Hendrickson, G. Christou, H. Ishimoto, J. Yoo, E. K. Brechin, A. Yamaguchi, E. M. Rumberger, S. M. J. Aubin, Z. Sun, G. Aromi, *Polyhedron* **2001**, *20*, 1479. c) S. M. J. Aubin, N. R. Dilley, M. W. Wemple, M. B. Maple, G. Christau, D. N. Hendrickson, *J. Am. Chem. Soc.* **1998**, *120*, 839.

23 The experiments[5a] for the Cole–Cole diagram based on a Debye model, which indicated a single relaxation process, also support the isolated spin system.

24 a) M. A. Gîrtu, C. M. Wynn, W. Fujita, K. Awaga, A. J. Epstein, *Phys. Rev. B* **2000**, *61*, 4117. b) S. P. Sellers, B. J. Korte, J. P. Fitzgerald, W. M. Reiff, G. Yee, *J. Am. Chem. Soc.* **1998**, *120*, 4662. c) J. E. Greedan, N. P. Raju, A. Maignan, C. Simon, J. S. Pedersen, A. M. Niraimathi, E. Gmelin, M. A. Subramanian, *Phys. Rev. B* **1996**, *54*, 7189.

25 J. A. Mydosh, *Spin Glasses: An Experimental Introduction*, Taylor and Francis, London, **1993**.

26 Theoretical calculation suggests that the Co^{II} ion in $[Co(X)_2(\mathbf{4NOpy})_4]$ has ^4E_g ground state. The axial ligands strongly interact with the t_{2g} orbitals of the Co^{II} ion to produce a large uniaxial ligand-field splitting parameter, Δ; the value of Δ increases with increasing the π-donor property of the axial ligands, leading to a large zero-field splitting parameter, $|D|$, by the spin–orbit coupling. However, this explanation is not consistent with the experimental results, because the π-donor property varies in the order of $NCO^- < NCS^- < Br^-$.

27 a) M. Murrie, S. J. Teat, H. Stoeckli-Evans, H.-U. Güdel, *Angew. Chem., Int. Ed.* **2003**, *42*, 4653. b) J. R. Galan-Mascaros, K. R. Dunbar, *Angew. Chem., Int. Ed.* **2003**, *42*, 2289. c) E. C. Yang, D. N. Hendrickson, W. Wernsdorfer, M. Nakano, L. N. Zakharov, R. D. Sommer, A. L. Rheingold, M. Ledezma-Gaeraud, G. Christou, *J. Appl. Phys.* **2002**, *91*, 7382. d) A. Caneschi, D. Gatteschi, N. Lalioti, R. Sessoli, L. Sorace, V. Tangoulis, A. Vindigni, *Chem. Eur. J.* **2002**, *8*, 286.

28 a) SIR 92: A. Altomare, G. Cascarano, C. Giacovazzo, A. Guagliardi, *J. Appl. Crystallogr.* **1993**, *26*, 343. b) DIRDIF99: P. T. Beurskens, G. Admiraal, G. Beurskens, W. P. Bosman, R. de Gelder, R. Israel, J. M. M. Smits, *The DIRDIF-99 Program System, Technical Report of the Crystallography Laboratory*, University of Nijmegen, The Netherlands, **1994**. c) *Crystal Structure 3.5.1: Crystal Structure Analysis Package*, Rigaku and Rigaku/MSC, 9009 New Trails Dr., The Woodlands, TX 77381, U.S.A. **2000–2003**.